Chemo and phototactic nano/microbots

Ayusman Sen,*[a] Michael Ibele,[a] Yiying Hong[a] and Darrell Velegol*[b]

Received 16th January 2009, Accepted 23rd March 2009
First published as an Advance Article on the web 21st July 2009
DOI: 10.1039/b900971j

One of the more interesting recent discoveries has been the ability to design nano/microparticles which catalytically harness the chemical energy in their environments to move autonomously. These "nanomotors" can be directed by externally applied magnetic fields, or optical and chemical gradients. Our group has now developed two systems in which chemical secretions from the translating micro/nanomotors initiate long-range, collective interactions among the particles *via* self-diffusiophoresis. Herein, we discuss two different approaches to model the complex emergent behavior of these particles, the first being a qualitative probability-based model with wide applicability, and the second being a more quantitative Brownian dynamics simulation specific to the self-diffusiophoretic phenomenon.

1 Introduction

One of the grand challenges in science is: *How can we master energy and information on the nano/microscale to create new technologies with capabilities rivaling those of living things?* We have initiated a study of emergent behavior and the consequent formation of organized material assemblies by using catalytic nano/micromotors.[1–7] Catalytic motors are a novel class of nano- and microscale materials that convert chemical to mechanical energy. Their collective behavior offers a means of using the free energy of chemical fuels to fabricate organized systems of particles. They may thus offer a route to functional assemblies that cannot be accessed by other means. Individually the motors move in a *random* direction according to physics that has been well-established by our groups.[3,8–10] But *collectively*, the motors give complex behaviors similar to the chemotaxis, phototaxis, or predator–prey phenomena normally seen only in biological systems.[9]

The construction of functional nano/microbots capable of emergent collective behavior requires the following design elements: (1) autonomous movement through catalysis; (2) control of directionality through chemical gradients; and (3) inter-motor communication *via* chemical signals. As discussed below, we have "proof of principle" examples of each of the above design elements, both separately and in combination.

2 Background

Several breakthroughs from our laboratory make the design of micro/nanobots based on catalytic motors possible. The first of these advances is our ability to fabricate catalytically active multi-metallic rods or aggregates. We have demonstrated that platinum/gold rods (2 μm length, 300–500 nm diameter) can "swim" by self-electrophoresis up to 20 μm s^{-1}.[1,3] Outside of biological systems, this was the first

[a]*Departments of Chemistry, The Pennsylvania State University, University Park, PA, 16802, USA. E-mail: asen@psu.edu*
[b]*Chemical Engineering, The Pennsylvania State University, University Park, PA, 16802, USA. E-mail: velegol@psu.edu*

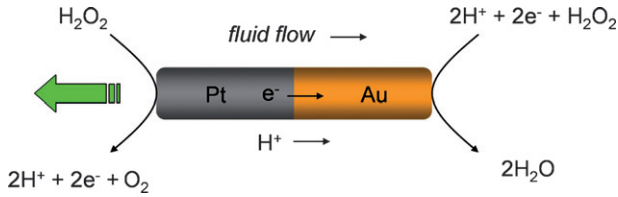

Fig. 1 Schematic illustrating self-electrophoresis. Hydrogen peroxide is oxidized to generate protons in solution and electrons in the wire on the platinum end. The protons and electrons are then consumed with the reduction of H_2O_2 on the gold end. The resulting ion flux induces an electric field and motion of the particle relative to the fluid, propelling the particle towards the platinum end with respect to the fluid.[3]

example of microscale objects moving by catalysis. They do this by catalyzing the decomposition of hydrogen peroxide (H_2O_2) (Fig. 1), and the rods move along their axis with platinum end forward, as our electrokinetic model predicts.[3,8,10,11] Several important capabilities have been added to the basic auto-mobile device. Among these are (1) steering; (2) the ability to carry cargo; (3) chemotaxis; and (4) collective behavior.

Steering of catalytic nanomotors

"Steering" capability is added by incorporating nickel (magnetic) stripes. The nanomotors can thus be "remote-controlled" by weak magnetic fields.[12]

We further demonstrated control over catalytic motors by designing platinum/gold structures with different geometries, such as "microgears" that rotate in hydrogen peroxide solutions (Fig. 2).[13] We have also expanded our work to include immobilized catalyst systems that can be used as micropumps. These silver/gold pumps (Fig. 3) are capable of "pumping" tracer particles due to the electrochemical decomposition of hydrogen peroxide (or other redox fuels[14]) on the bimetallic surface.[3,8,10]

Cargo-carrying catalytic nanomotors

We were able to attach a prototypical cargo: polystyrene microspheres to platinum/gold nanomotors, which can then be transported (Fig. 4).[15] Assuming

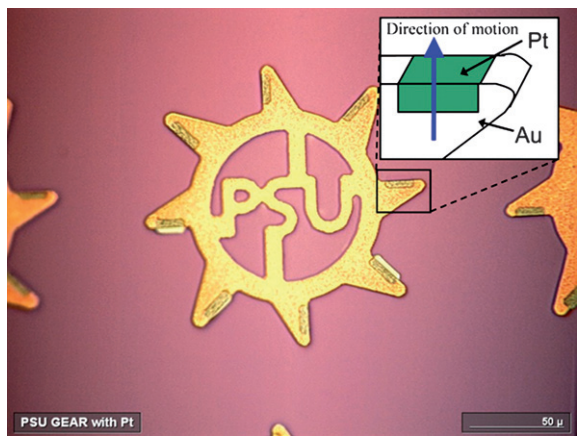

Fig. 2 100 μm diameter gold "microgears" with platinum "teeth" can rotate ~360° s^{-1} in aqueous hydrogen peroxide systems.[13]

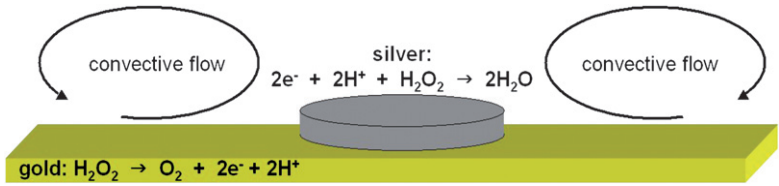

Fig. 3 A catalytic micropump consisting of a silver disk on a gold substrate. The electrochemical decomposition of hydrogen peroxide establishes a weak electric field. This field causes tracer particles to migrate *towards* or *away* from the silver depending on their *surface charge*. Particles migrating towards the silver follow *electroosmotic convection* (arrows) near the catalyst surface.[8]

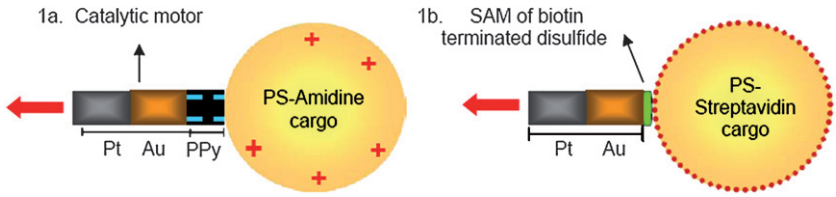

Fig. 4 Cargo attachment by (a) electrostatic interaction between the negative polypyrrole (PPy) end of a platinum/gold/polypyrrole motor and a positively charged polystyrene (PS)–amidine micro-sphere and (b) biotin–streptavidin binding between the gold tips of platinum/gold rods functionalized with a biotin-terminated disulfide and streptavidin-coated cargo.[15]

a cargo-independent motive force, the speeds are inversely proportional to the Stokes resistance, which we compute using a double-layer boundary integral equation. Magnetic Ni segments incorporated into the rods quench the rotational diffusion (and biased rotation) in the presence of an external magnetic field, making such motors ideal for cargo pick-up and delivery. Chemotaxis of the rods was also used to transport cargo to a region of high hydrogen peroxide concentration (see below). Many interesting applications can be envisioned for such cargo bearing motors in the mesoscale. For instance, this provides a simple method for concentrating colloids against their entropic tendency to disperse.

Chemotaxis of catalytic nanomotors

We have discovered that the platinum/gold nanorods exhibit chemotaxis (Fig. 5),[9] traditionally defined as the movement of "organisms" toward or away from a chemical attractant or toxin by a biased random walk process.[16] Again, this is the first example outside living systems. Our work also reveals that chemotaxis does not require a sophisticated "temporal sensing" mechanism commonly attributed to small organisms. Rather, the nanoparticles move up a fuel gradient as a result of faster "powered diffusion" in higher fuel concentrations; a straightforward extension is movement towards or away from a signaling molecule.[9] The signaling molecule could be a promoter or an inhibitor of the catalytic reaction. This behavior provides a novel way to direct particle movement towards specific targets, even while allowing them to sample a large region of fluid by powered diffusive motion. This discovery is potentially important in the design of "smart" autonomous nano-robots, which could move independently in the direction they are needed, perhaps by harvesting energy from glucose or other abundant fuels in biological or organic systems. Chemotaxis also offers a novel method of sorting and separating particles of similar mass and size. Only those particles that are catalytically active move in response to the chemical gradient. From a fundamental standpoint, our work could be the starting point for the design of new motors for collective functions, such as catalytically

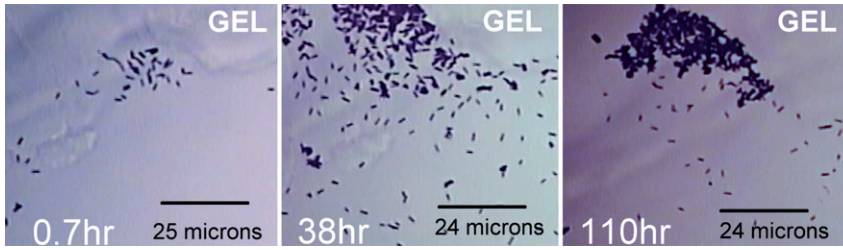

Fig. 5 The changing distribution of platinum/gold rods in a hydrogen peroxide concentration gradient. The gel (soaked in 30% hydrogen peroxide) appears in the upper left part. The images were taken at 0.7 h, 38 h, and 110 h.[9]

driven swarming and pattern formation. This aspect of our work is elaborated in the next section.

Results and discussion

Collective behavior of particles undergoing self-diffusiophoresis

The biological world is rife with examples of organisms using chemotaxis to communicate between spatially isolated cells and accomplish collective tasks. For instance, the unicellular slime mold amoebae *Dictyostelium discoideum* secretes a signaling chemical, 3′-5′-cyclic adenosine monophosphate (cAMP), into the environment when stressed. Nearby slime molds detect this chemical, respond by secreting additional cAMP, thus amplifying the signal, and move up the global cAMP chemical gradient to assemble as a multi-cellular fruiting body.[16]

The key aspect of this collective behavior among slime molds is that the organisms both produce and are translated by the cAMP chemical gradient. We have recently developed a synthetic system operating on that very same principle. Namely, we have observed that micrometer-sized silver chloride (AgCl) particles move under UV illumination in deionized water *via* self-diffusiophoresis (Fig. 6).[17] The AgCl particles move in response to self-imposed salt gradients, a phenomenon which although obviously mechanistically different to the slime mold system, exhibits many qualitative similarities. Like the *Dictyostelium discoideum*, each AgCl particle secretes chemicals (in this case, ions) as it moves, to which the other particles respond. Over the course of a few minutes, this causes the AgCl particles to organize into discrete regions with higher particle concentrations, or "schools," a pattern that fits the known 2D model of the slime mold's behavior (Fig. 7).[17,18]

Although oxygen is produced during the dissolution of the AgCl, a bubble propulsion mechanism for these particles is unlikely because bubble evolution is not observed over the course of the experiment due to the relatively slow reaction rate. Bubble propulsion also cannot account for the long range interaction between particles. Although particle organization from optical trapping is well known, it is unlikely to be the case in this system since the phenomenon was not observed for photo-insensitive polystyrene colloids of similar refractive index. Furthermore, the map of the UV light intensity produced by our microscope was roughly Gaussian in nature and contained no "hot spots." If such a beam resulted in optical trapping, particles would be shuttled to the beam center and not form dozens of isolated "schools".

Also, because diffusiophoresis[19,20] is a physical phenomenon, even photo-inactive silica particles respond to the chemical secretion of the AgCl by swimming towards and surrounding individual AgCl particles, a predator–prey behavior not unlike that of neutrophils (Fig. 8).[21] This ability to fabricate systems of synthetic particles which can interact over relatively long distances demonstrates new design principles for

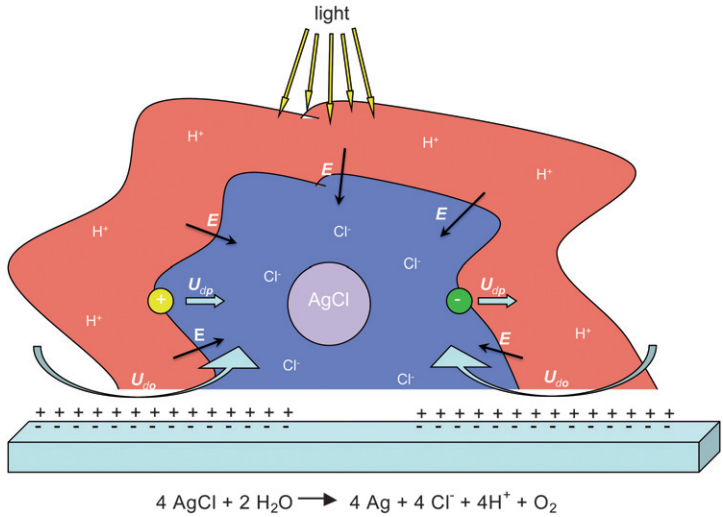

Fig. 6 Photochemistry of silver chloride. Briefly, the photolysis of a AgCl particle results in the formation of H^+ and Cl^- ions. The H^+ diffuses out significantly faster than the Cl^-, resulting in an electric field. This electric field acts (a) phoretically on any other nearby charged particles (shown as yellow and green spheres) giving them a velocity U_{dp}; (b) osmotically on ions in the double layer of any nearby wall surfaces to create a fluid flow near the surface U_{do}; and (c) phoretically back on the particle itself in the case of an asymmetric field.[19,20] When there is a high enough concentration of particles, the particles move cooperatively in response to each others' ion gradients to form macroscopic schools (Fig. 7).

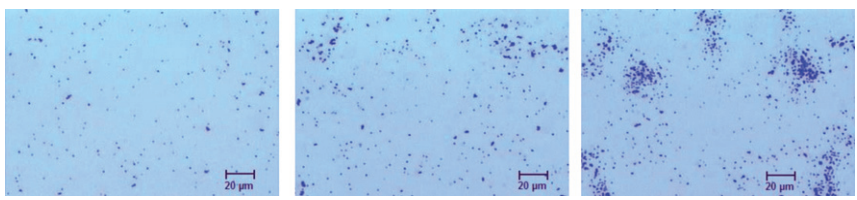

Fig. 7 AgCl particle "schooling". AgCl particles in deionized water (left) before UV illumination, (centre) after 30 s of UV exposure, and (right) after 90 s.[17]

"intelligent" synthetic nano/micromachines that function collectively. There are many possible ways of designing ion-producing nano/microparticles, including particles with attached catalysts or enzymes that form ions as products. These particles should then interact with each other or with inert nano/microparticles through their ionic products. In addition, the design principle allows the coordinated movement of dissimilar particles that are not attached to each other, making it easier to transport and deliver cargo at designated areas.

A simple model for collective behavior

In order to explore the dynamics of such collective behavior among individual particles, a simple simulation was developed from first principles. Let us first consider that the particles (white circles in Fig. 9a) are infinitesimally small and each of the (N) particles occupies a discrete site (x, y) on a finite two-dimensional square lattice with periodic boundaries. The particles are then allowed to "hop" to one of their four nearest neighbor sites with some probability every time-step. There is no limit to the number of particles which can occupy any one site. Purely Brownian motion,

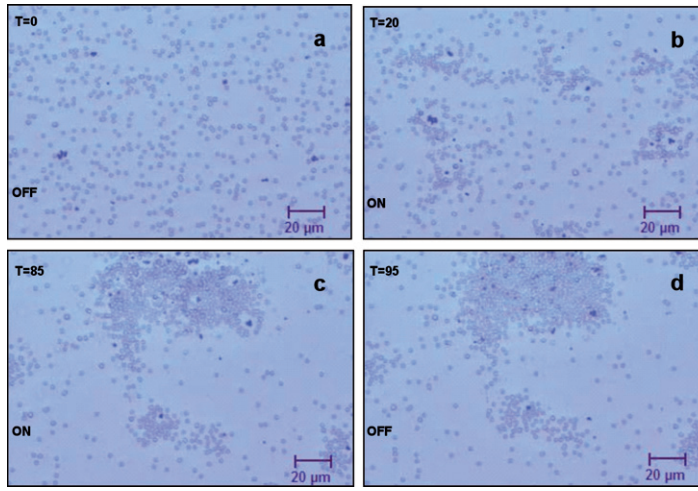

Fig. 8 AgCl particles ~7 μm in diameter (darker objects) have been mixed with 2.34 μm silica spheres and placed in deionized water (a). When illuminated with UV light (b and c) the silica spheres actively seek out the AgCl particles and surround them. While the UV light is on, an exclusion zone is seen around the AgCl particles; this exclusion zone disappears when the UV light is turned off (d). Times in seconds are listed in the upper left hand corner. Status of the UV light is listed in the bottom left.[17]

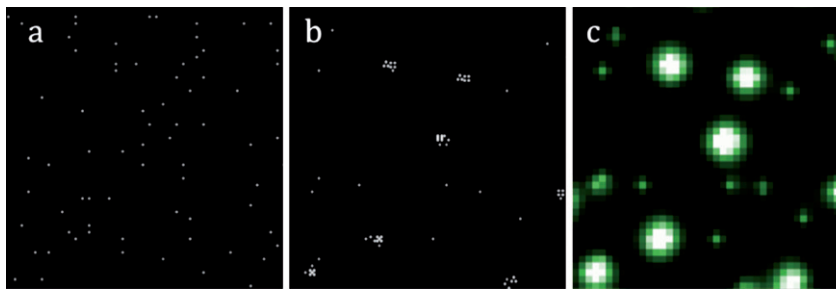

Fig. 9 A typical simulation of particle collective behavior. Image represents one-fourth of the total simulation space and has been zoomed in for clarity. (a) Initially randomly distributed particles. (b) Particles after 2000 times-steps. (c) A plot of the chemical values of every lattice site at 2000 time-steps. Brighter shades of green approaching white indicate higher chemical concentrations.

for instance, can then be considered as a uniform hopping probability λ_B for every particle in each of the four directions.

In the AgCl system described above, particles interact by secreting chemical signals into their environments. These chemical signals diffuse out into the solution over time, allowing for long range interactions. To incorporate such interactions into our model, we propose that each lattice site also has a numerical "concentration" value ($C_{x,y}$) associated with it (Fig. 9c). This value is initially zero for all sites. During the simulation, for each time-step, the concentration value of the lattice site is increased in proportion (by a factor of a in eqn (1)) to the number of particles currently occupying that site ($n_{x,y}$).

The concentration value associated with each lattice site is then allowed to "diffuse" outward to neighboring lattice sites—*i.e.*, the concentration value from one site gets redistributed to its four nearest neighbors in a manner which is dictated by Fick's Second Law. Specifically, each time-step every cell loses some small

portion of its current chemical concentration [$D \times C_{x,y}(t)$] to each of its four nearest neighbors, and gains a small portion of their chemical in return. In addition to this strict diffusion, each lattice site loses some small proportion (b in eqn (1)) of its total chemical value every time-step. This small loss is included to allow the two-dimensional simulation to more closely approximate conditions found in real systems which are three-dimensional. More specifically, it helps account for the fact that any chemical signal produced by the particles will not only diffuse in the two-dimensional field of view, but also some portion of the chemical will diffuse into the bulk solution and be lost. Therefore, in the simulation, the chemical concentration of any site ($C_{x,y}$) at any time-step ($t + \Delta t$) is given by eqn (1), where a and b are constants and are members of $[0, \infty]$ and [0,1], respectively.

$$\underbrace{C_{x,y}(t+\Delta t)}_{New\ \ Conc.} = \underbrace{(1-b)}_{Bulk\ \ Loss} \left\{ \underbrace{C_{x,y}(t)}_{Original\ \ Conc.} + \underbrace{an_{x,y}}_{Chemical\ \ Production} + \underbrace{D\left[C_{x+1,y}(t) + C_{x-1,y}(t) + C_{x,y+1}(t) + C_{x,y-1}(t) - 4C_{x,y}(t)\right]}_{Diffusion} \right\} \quad (1)$$

The final component of the simulation is then just the addition of a bias which causes the particles to have a preference to hop towards regions with higher chemical values. This bias is introduced as extra hops (in addition to the Brownian hops) in the x and the y direction which depend on the gradient of chemical value across the particle's host site. To do this, the gradient in the chemical value across the host site of a given particle is evaluated in both the x and y directions (ψ_x and ψ_y). Individual hops are then taken in the x and y directions with probabilities (λ_x and λ_y) proportional to the gradients in those respective directions, as depicted by eqn (2) and (3). Here α is a constant representing the sensitivity to the chemical gradient. The directions of these two hops are determined by the signs of ψ_x and ψ_y, and both λ_x and λ_y are of course constrained to be less than one by an appropriate choice of α.

$$\psi_x = C_{x+1,y}(t) - C_{x-1,y}(t) \quad (2a)$$

$$\psi_y = C_{x,y+1}(t) - C_{x,y-1}(t) \quad (2b)$$

$$\lambda_x(t) = \alpha|\psi_x| \quad (3a)$$

$$\lambda_y(t) = \alpha|\psi_y| \quad (3b)$$

In the physical world, this gradient-related hopping bias may take a variety of forms. It may correspond to a diffusiophoretic force on a particle (*e.g.*, the AgCl system), a chemotactic tendency to travel up fuel gradients (*e.g.*, catalytic nanorods in H_2O_2 gradient), or any one of a number of complex signaling pathways found in biological systems.

As we can see from Fig. 10(a)–(e), our model shows that a number of factors can influence the ability of these modeled particles to form collective schools. In each of these graphs, one parameter of the system was changed, holding all other parameters constant. The simulation was run for 1000 time-steps, and the propensity of the particles to be in schools at $t = 1000$ was plotted. Here the schooling propensity is defined as the proportion of particles occupying lattice sites which are occupied by four or more particles (an arbitrary cut-off) at the end of the simulation. Each data point represents ten simulations with error bars of one standard deviation.

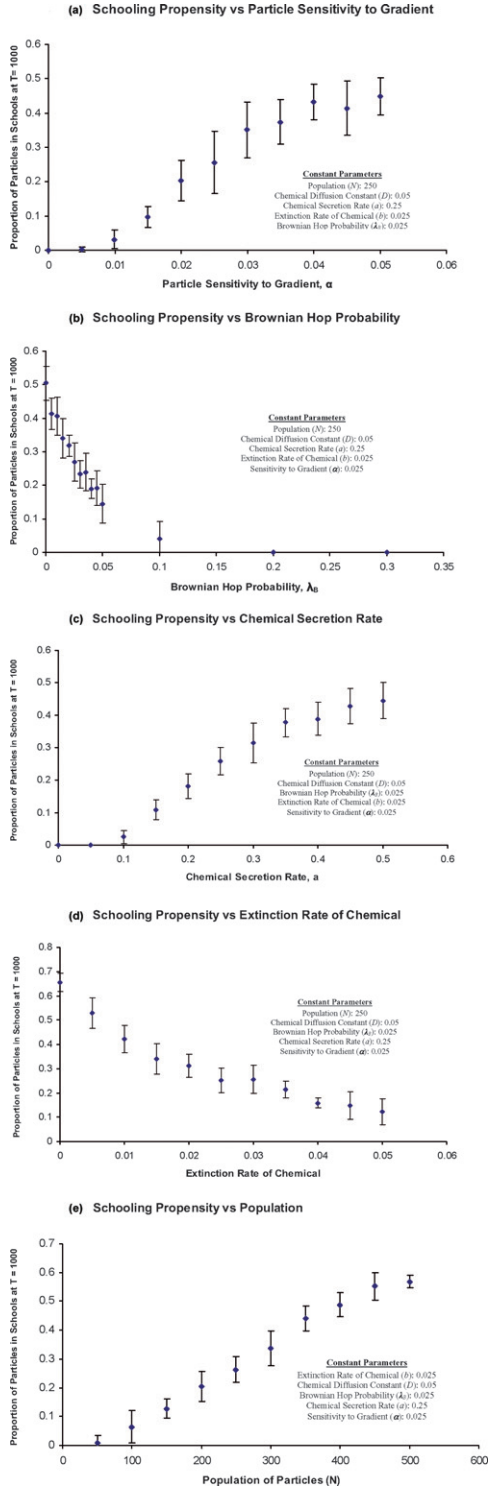

Fig. 10 Plots summarizing the particle location statistics for the qualitative probability-model of collective behavior. In each graph, the proportion of particles residing in lattice sites with

Certainly, the most obvious variable of note is the sensitivity α to the chemical gradient. For a given gradient, the particle's propensity to hop up the gradient (Fig. 10(a)) must be large enough to overcome the randomizing effects of Brownian motion (Fig. 10(b)). Similarly, the steepness of the chemical gradient also plays a role. This can be achieved by increasing the "secretion rate" a of the chemical from the colloids, or by lowering the "extinction rate" b of the chemical from the environment (Fig. 10(c) and 10(d)).

The number density of particles in the system (Fig. 10(e)) is also an important parameter. For small populations of particles, the inter-particle spacing is relatively large. As a result, the chemical signal from one particle becomes significantly diluted before reaching its nearest neighbor. The resultant gradient is therefore gentler, and thus the hopping probability (λ) of the second particle towards the first is relatively small.

Photo-patterning of particles

Thus far, our discussion of self-diffusiophoresis has assumed a uniform illumination of the ion-producing photoactive particles. Yet this need not be the case. Recently we have observed that an asymmetric gradient of light impinging on photocatalytic particles can result in pattern formation. An example is shown in Fig. 11 where silica–silver (SiO_2–Ag) Janus particles move away from the UV illuminated area due to a chemical gradient created by a photolysis reaction.

In this example, the SiO_2–Ag Janus particles, with a 60∼80 nm thickness of Ag evaporated onto one side of the SiO_2 (d, 2.34 μm), are placed in 0.5% H_2O_2 solution in a sealed imaging chamber. A photolysis reaction between Ag and H_2O_2 is initiated upon UV irradiation through the microscope objective, producing Ag^+ and OOH^- ions. The differential diffusion coefficients of these ions induce an electric field localized at the particle length scale, which in turn causes the individual particles to move by the mechanism of self-diffusiophoresis.[19,20] A macro-scale ion gradient is also produced corresponding to the different UV illumination levels within the system. This results in a circular ion gradient, centered on the microscope objective's focal point, causing the particles to move away from the highest ion concentration area, *i.e.*, the center of the field. The action is again emergent, analogous to that of quorum sensing,[22,23] where a threshold concentration of the signaling chemical is required to trigger the migration of the organisms. We found that a minimum particle density of 10^6 mL^{-1} is required in our SiO_2–Ag phototaxis experiment to overcome the randomizing effect of Brownian motion for an observation time of 1–2 h.

Control experiments performed without H_2O_2 showed a slight accumulation of particles at the light spot after 24 h, indicating the existence of a thermal effect, which is in the opposite direction to the phototactic effect and takes longer. The negative phototaxis (*i.e.*, a hole at the UV spot) of SiO_2–Ag Janus particles in the presence of H_2O_2 is significant because the particles have to *overcome* the thermal effect to be able to escape from the high UV intensity region.

Earlier in this paper we described a general model for the examination of collective particle interactions. Although the general nature of the model allows for high throughput and wide application, its quantitative predictive power is limited. Therefore, we have developed a second, independent model which specifically addresses particle collective interactions from a standpoint of self-diffusiophoresis.

This system-specific Brownian Dynamic Simulation (BDS)[24] addresses the diffusiophoretic motion of settled particles close to a surface, a diffusioosmotic motion due to the underlying surface, and a Brownian motion of the particles (eqn (4)).

four or more total particles at $T = 1000$ is plotted *vs.* one independently modified parameter. Each data point represents ten simulations with error bars of one standard deviation.

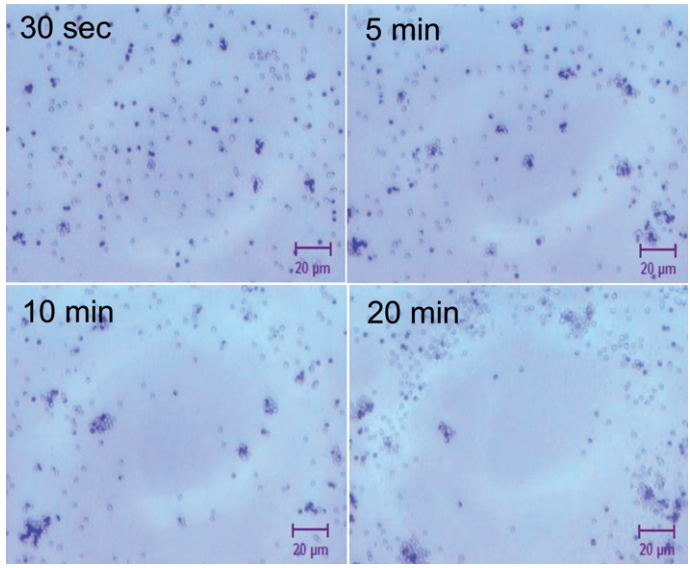

Fig. 11 Time-lapse images show the phototactic process of SiO_2–Ag Janus particles in 0.5% H_2O_2 under the irradiation of a circular spot by ultraviolet light.

Just as before, we modeled N particles in 2 dimensions, in a fluid over an area ($A = L \times L$). However, in this model, particle positions were treated as floating-point locations on top of a 100 × 100 integer grid which contained the chemical concentration data. Each grid site corresponds to a 30 μm^2 area of fluid. Also, in this model the particle motions were treated not as hops of unit distance with finite probability but as hops of variable distance which occur every time-step.

To simplify the applicable hydrodynamic equations, spherical particles were assumed, and any change in the hydrodynamics near the surface due to lubrication or multi-body effects was neglected. The overall change in position, Δx, for a particle in a given time-step can then be described as a superposition of the displacements caused by the diffusiophoretic velocity (U_{dp}), the diffusioosmotic velocity (U_{do}), and the Brownian diffusion (Δx_B), as seen in eqn (4).

$$\Delta x = U_{dp}\Delta t + U_{do}\Delta t + \Delta x_B \tag{4}$$

The diffusiophoretic velocity U_{dp} of a particle with a thin double layer is given by eqn (5),

$$U_{dp} = \frac{2Ze}{\kappa^2\eta}\left[\left(\frac{D_+ - D_-}{D_+ + D_-}\right)\zeta_p - \frac{2kT}{Ze}\ln\left(1 - \gamma_p^2\right)\right]\nabla C \tag{5}$$

where Z is the valence of the ions; e is the proton charge; κ^{-1} is the solution Debye length (178 nm for water in equilibrium with air); ζ_p is the particle ζ-potential (ζ_p, approx. −30 mV for most of our particles); η is the solution viscosity (0.89 cP for water at 25 °C); $\gamma_p = \tanh(Ze\zeta_p/4kT)$; and ∇C is the concentration gradient of the ions, which by electroneutrality must have the same bulk concentration at all locations. The diffusion coefficients are known at 25 °C for the positive (Ag^+, $D_+ = 1.65 \times 10^{-9}$ m^2 s^{-1})[25] and negative (OOH^-, $D_- = 0.3 \times 10^{-9}$ m^2 s^{-1}) ions.[26] The diffusioosmotic velocity (U_{do}) of the fluid carrying the particles, where this movement is due to the underlying surface, is given by eqn (6), where the wall ζ-potential (ζ_w, approx. −70 mV) is considered.

$$U_{\mathrm{do}} = -\frac{2Ze}{\kappa^2\eta}\left[\left(\frac{D_+ - D_-}{D_+ + D_-}\right)\zeta_{\mathrm{w}} - \frac{2kT}{Ze}\ln\left(1 - \gamma_{\mathrm{w}}{}^2\right)\right]\nabla c \tag{6}$$

The illumination spot was defined as having a radius of 10 grid points. All particles that were within the central laser spot produced Ag^+ and OOH^- ions at a turnover rate of 9.4 per catalytic site per second (catalytic site size ~ 0.25 nm^2), which was determined from separate experiments. No account was taken to assess changes in reaction rate with H_2O_2 concentration or illumination power. And the change in H_2O_2 concentration over the time span of our experiment was negligible due to its relatively high concentration. The particles were assumed to be "point sources" producing these ions, which were then allowed to diffuse in two dimensions by Fick's second law. From the final concentration field at each time step, we calculated ∇c.

The results show that a hole develops in the center of the UV spot over time. We use a relatively low particle density ($N = 1000$) to show the time-wise effect. As can be seen in Fig. 12, the hole grows over time, but stops growing after about 5 h ($\tau = 200$). The size of the hole is dependent on the UV spot size. In the real experiments, thermal effects take over after 4–6 h and cause aggregation of particles. Thus, we focus on the phototactic effect shown within 1–2 h.

In order to simulate the emergent behavior, we set the reaction time to $\tau = 50$ ($= 75$ min), which is about the time required to observe the phototactic effect experimentally ($\sim$1 h). We vary the particle number and find that below $N = 1000$, the phototactic effect is no longer observed (Fig. 13). The threshold is determined by the balance between the reaction rate (how fast the ion gradient builds up) and the dissipation rate, which is mainly contributed by Brownian diffusion. Knowing that the actual UV spot is 600 μm in diameter, $N = 1000$ in the model translates to a particle density of 2×10^5 mL^{-1}. This is in agreement with our experimental observation that a minimum particle density of 10^6 mL^{-1} is needed for the patterning to occur.

Conclusion

We have engineered the first examples of nano/micro-objects outside living systems that move autonomously by converting chemical energy into mechanical force. With

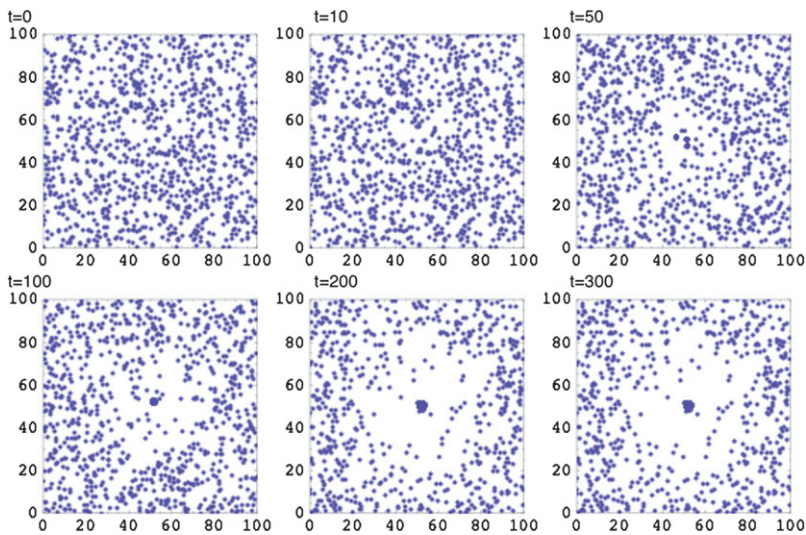

Fig. 12 Brownian dynamics simulation shows the development of the central hole over time at a particle number of $N = 1000$.

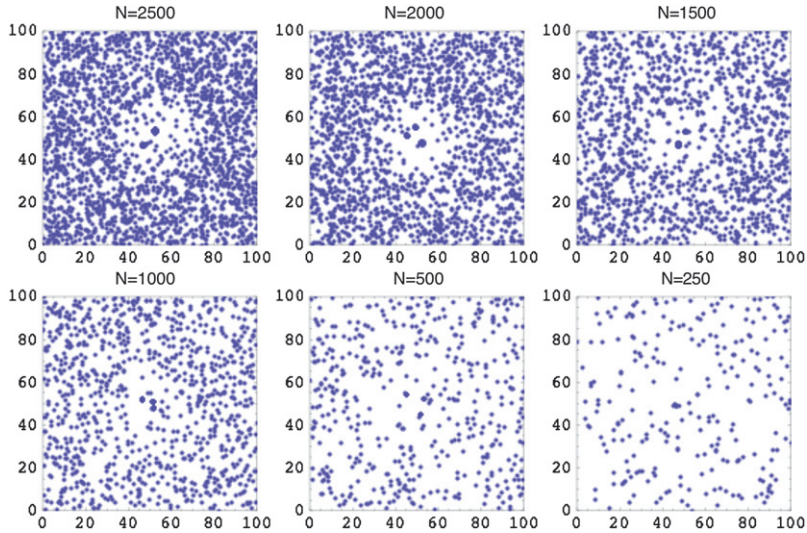

Fig. 13 Brownian dynamics simulation shows how particle density affects the phototactic behavior.

very little "information" input (in the form of chemical gradients), these objects begin to display emergent collective behaviors that were thought to lie solely in the realms of biology. Liberated of the usual biological constraints, we now have an unprecedented opportunity to probe the ultimate limits of self-organization in these dynamic systems. If successful, our work should lead to novel design paradigms for assembly and patterning of particles.

Acknowledgements

We thank Dr Thomas Mallouk, Dr Vincent Crespi and Dr Paul Lammert for helpful discussions. The work is funded by the Penn State Center for Nanoscale Science (NSF-MRSEC, DMR-0820404), NSF NIRT CTS-0506967, and NSF CBET-0651611. Support was also given by the NSF-supported Penn State University's National Nanotechnology Infrastructure Network (NNIN).

References

1 W. F. Paxton, K. C. Kistler, C. C. Olmeda, A. Sen, S. K. St. Angelo, Y. Cao, T. E. Mallouk, P. E. Lammert and V. H. Crespi, *J. Am. Chem. Soc.*, 2004, **126**, 13424.
2 (*a*) S. Fournier-Bidoz, A. C. Arsenault, I. Manners and G. A. Ozin, *Chem. Commun.*, 2005, 441; (*b*) G. A. Ozin, I. Manners, S. Fournier-Bidoz and A. Arsenault, *Adv. Mater.*, 2005, **17**, 3011.
3 W. F. Paxton, P. T. Baker, T. R. Kline, Y. Wang, T. E. Mallouk and A. Sen, *J. Am. Chem. Soc.*, 2006, **128**, 14881.
4 J. Vicario, R. Eelkema, W. R. Browne, A. Meetsma, R. M. La Crois and B. L. Feringa, *Chem. Commun.*, 2005, 3936.
5 N. Mano and A. Heller, *J. Am. Chem. Soc.*, 2005, **127**, 11574.
6 J. Howse, R. A. L. Jones, A. Ryan, T. Gough, R. Vafabakhsh and R. Golestanian, *Phys. Rev. Lett.*, 2007, **99**, 048102.
7 W. F. Paxton, S. Sundararajan, T. E. Mallouk and A. Sen, *Angew. Chem., Int. Ed.*, 2006, **45**, 5420.
8 T. R. Kline, W. F. Paxton, Y. Wang, D. Velegol, T. E. Mallouk and A. Sen, *J. Am. Chem. Soc.*, 2005, **127**, 17150.
9 Y. Hong, N. M. K. Blackman, N. D. Kopp, D. Velegol and A. Sen, *Phys. Rev. Lett.*, 2007, **99**, 178103.

10 T. R. Kline, J. Iwata, P. E. Lammert, T. E. Mallouk, A. Sen and D. Velegol, *J. Phys. Chem. B*, 2006, **110**, 24513.
11 W. F. Paxton, A. Sen and T. E. Mallouk, *Chem.–Eur. J.*, 2005, **11**, 6462.
12 T. R. Kline, W. F. Paxton, T. E. Mallouk and A. Sen, *Angew. Chem., Int. Ed.*, 2005, **44**, 744.
13 J. Catchmark, S. Subramanian and A. Sen, *Small*, 2005, **1**, 202.
14 M. Ibele, Y. Wang, T. R. Kline, T. E. Mallouk and A. Sen, *J. Am. Chem. Soc.*, 2007, **129**, 7762.
15 S. Sundararajan, P. E. Lammert, A. W. Zudans, V. H. Crespi and A. Sen, *Nano Lett.*, 2008, **8**, 1271.
16 (*a*) P. Devreotes and C. Janetopoulos, *J. Biol. Chem.*, 2003, **278**, 20445; (*b*) H. C. Berg, *Phys. Today*, 2000, 53; (*c*) J. Adler and W. W. Tso, *Science*, 1974, **184**, 1292; (*d*) R. M. Macnab and D. E. Koshland, *Proc. Natl. Acad. Sci. U. S. A.*, 1972, **69**, 2509.
17 M. Ibele, T. Mallouk and A. Sen, *Angew. Chem., Int. Ed.*, 2009, **48**, 3308.
18 U. Wilensky, 1997. *NetLogo Slime Model from the Center for Connected Learning and Computer-Based Modeling*, Northwestern University, Evanston, IL http://www.ccl.northwestern.edu/netlogo/models/Slime.
19 J. L. Anderson, *Annu. Rev. Fluid Mech.*, 1989, **21**, 61.
20 S. Dukhin, and B. Derjaguin, *Electrokinetic Phenomena*, John Wiley, New York, 1974.
21 D. Billadeau, *Nat. Immunol.*, 2008, **9**, 716.
22 S. R. Chhabra, B. Philipp, L. Eberl, M. Givskov, P. Williams and M. Cámara, *Top. Curr. Chem.*, 2005, **240**, 279.
23 P. Devreotes, *Science*, 1989, **245**, 1054.
24 W. B. Russell, D. A. Saville and W. R Schowalter, *Colloidal Dispersions*, Cambridge University Press, 1989. Sections 3.5 and 3.6 outline how the BDS is obtained from the Langevin equation.
25 *CRC Handbook of Chemistry and Physics*, 87th edn., ed. D. R. Lide, Taylor & Francis, Boca Raton, New York, 2006–2007.
26 T. R. Kline and A. Sen, *Langmuir*, 2006, **22**, 7124.